JMEPEG (2000) 9:700–709

Influence of Nonmetallic Inclusion Characteristics on the Mechanical Properties of Rail Steel

S.K. Dhua, Amitava Ray, S.K. Sen, M.S. Prasad, K.B. Mishra, and S. Jha

(Submitted 20 December 1999)

An extensive investigation has been carried out on six commercial heats of pearlitic rail steel to study the influence of nonmetallic inclusion characteristics on the tensile, fatigue, and fracture toughness properties. The steels investigated were made through the basic oxygen furnace (BOF)-continuous casting route and rolled in the rail and structural mill into 90 kg/mm^2 ultimate tensile strength (UTS) grade rails. While tensile properties (yield strength [YS], UTS, and elongation) of the rail steels investigated were found to be insensitive to inclusion type and volume fraction at their present level (0.23 to 0.45%), the fracture toughness and high-cycle fatigue properties were found to be inclusion sensitive. The fracture toughness values of the steels were found to range between 42.33 and 49.88 MPa $\sqrt{m}$; higher values, in general, were obtained in heats exhibiting lower volume fractions (0.15 to 0.19%) of sulfide inclusions. The high-cycle fatigue limit, *i.e.*, stress corresponding to 10^7 cycles, was found to be higher in cleaner steels, particularly in those with lower volume fractions of oxide inclusions. This phenomenon was corroborated by scanning electron microscopy (SEM) observations of fracture surfaces, where oxide inclusions in particular were found to be instrumental in crack initiation. Although fatigue life did not show any direct correlation with the volume fraction of sulfides, elongated MnS inclusions were sometimes observed at crack initiation sites of fatigue-tested specimens.

Keywords mechanical properties, nonmetallic inclusions, pearlitic structure, railway steel

1. Introduction

In present day situations, rails have to withstand severe service conditions and greater stresses owing to higher axle loads, quantum increase in freight volume, and high operating speeds.[1] Consequently, rails in service are subject to thousands of stress reversals that may eventually lead to fatigue cracking and fracture. This trend is likely to continue in the coming century, and hence, expectations for superior rail quality and improved performance are likely to increase further. The basic properties that govern rail performance are resistance to wear, fatigue, plastic deformation, and levels of residual stress and weldability. While increase in wear resistance and resistance to plastic deformation can be achieved by increasing the hardness of rail steels and through improvements in lubrication and grinding technologies, attainment of superior fatigue resistance would undoubtedly involve a thorough understanding of inclusion characteristics and fracture toughness properties.[2] Nonmetallic inclusions (NMI), which constitute inseparable species of extraneous particulate matter in steels, are known to profoundly influence the strength, toughness, and fatigue properties. These NMI could be "indigenous," *i.e.*, formed in liquid steel as consequences of deoxidation reactions, or "exogenous," *i.e.*, of extraneous origin.[3] Although indigenous inclusions such as sulfides and oxides are commonly observed in steels, the occurrence of exogenous inclusions is comparatively rare and may be attributed to entrainment of slag and/or refractories. While the deleterious influence of elongated sulfide inclusions is well known on the impact toughness of steels, its role on fatigue and fracture toughness behavior is not clearly understood. Fatigue, on the other hand, is known to be effected by the presence of hard, brittle, and nondeformable types of oxide inclusions owing to their stress-raising propensity. The role of such inclusions is therefore extremely vital for the performance of rail steels, since fatigue cracking constitutes a major mechanism of failure in the railroad industry.[4] Inclusions with a low deformability index tend to induce fatigue in two ways: (1) by directly nucleating cracks during service owing to their inability to transduce stresses in the steel matrix and (2) by possibly introducing microcracks at the steel/inclusion interface during working. These microcracks may eventually culminate in fatigue failure by propagation during service. Although scatter in the fatigue properties of most steels has been attributed to NMI, establishment of direct relationships between NMI content, fatigue, and fracture toughness properties is still elusive and continues to be an area of exploration. It is in this context that an extensive investigation has been carried out to study the effects of NMI characteristics on the tensile, fatigue and fracture toughness properties of commercially produced pearlitic rail steel.

2. Experimental

For conducting the investigation, six industrial heats with variations in sulfur and silicon were chosen. The steels were made through basic oxygen furnace (BOF)-continuous casting route and rolled in the rail and structural mill into 90 kg/mm^2 ultimate tensile strength (UTS) grade rails. During steel making,

S.K. Dhua, Amitava Ray, S.K. Sen, M.S. Prasad, K.B. Mishra, and **S. Jha**, Physical Metallurgy Group, Research & Development Centre for Iron & Steel, Steel Authority of India Limited, Ranchi-834002, India.

deoxidation was effected in the ladle through additions of silicomanganese and aluminum, while argon purging was also performed to ensure temperature homogeneity and inclusion removal. The molten steel was then continuous cast in a four-strand bloom caster of 320 × 360 mm mold size. The casting was carried out at a speed of 0.6 to 0.75 m/min. The cast blooms were heated in a pusher-type reheating furnace and rolled subsequently in the rail and structural mill into 60 kg/m rail sections. The rolled rails were slowly cooled in pits to facilitate hydrogen removal.

From each rail steel heat, two samples (1.5 m length each) were obtained for preparation of test specimens. From these samples, transverse sections of approximately 12 to 15 mm thicknesses were cut and machine ground for macrostructural examination and sulfur printing. For sulfur printing, a 2% aqueous solution of sulfuric acid was used, while for macroetching, the specimens were immersed for 15 to 20 minutes in an aqueous solution of 50% HCl maintained at around 70 °C.

Optical microscopic examinations were conducted on specimens obtained from the grip portion of round tensile test pieces machined from the "head" region of rails. The longitudinal sections of metallographic specimens were examined in polished and unetched condition for observation of inclusion characteristics. Microstructural examination of phases, however, was carried out on nital (2 mL HNO_3 in 98 mL ethyl alcohol)-etched transverse sections of the same metallographic specimens at 500× magnification. Concurrently, etched metallographic specimens were examined at higher magnifications (5000 and 10,000×) through scanning electron microscopy (SEM) to observe pearlite resolution. The pearlite interlamellar spacings in each specimen were determined from SEM micrographs by linear intercept measurements.

Quantitative metallographic studies on NMI were conducted in a LEICA (LEICA Imaging Systems, Cambridge, United Kingdom) make "Quantimet-600" model image analysis system to determine the volume fractions of various inclusion species present. Parallel, microprobe analyses were conducted in a JEOL (Japan Electron Optics Ltd., Tokyo) make "JCXA-733" model electron-probe microanalyzer (EPMA) to determine inclusion chemistry.

Tensile tests were carried out on 10 mm gauge diameter round specimens in a 25 ton "Instron-1273" (Instron Limited, High Wycombe, Buckinghamshire, England) model universal testing machine in accordance with ASTM standard designation E 8M-96. The test specimens were obtained from the "head" region of rails and machined in the longitudinal direction. The location and dimensions of the test pieces are shown in Fig. 1(a) and (b), respectively. During testing, a 50 mm gauge length extensometer was used and a crosshead speed of 1 mm/min was maintained. For each rail heat, three specimens were tested and average values were reported for yield strength (YS), ultimate tensile strength (UTS), and elongation percent.

High-cycle fatigue tests of rail samples were carried out on longitudinal orientation cylindrical specimens prepared from the head portion of rails. The geometry of a typical test specimen is shown in Fig. 2. High-cycle fatigue testing was carried out in an Avery Denison (Avery Denison, Leeds, England) make "Bend Fatigue" type testing machine at stress levels ranging from 3 to 4.5 N m. At each stress level, at least four specimens were tested and the cycles undergone prior to failure were recorded. The cycles endured by a particular batch of specimens at a given stress level was taken as the average of three close values. The nominal stress on the specimen was calculated from the applied bending moment by using the following formula:[5]

$$S = \frac{32 \times M \times 1000}{\pi \times (D)^3}$$

where

S = nominal stress, Mpa;
M = bending moment applied, N m; and
D = gauge diameter of specimen, mm

The fatigue limit was then determined from the plotted stress (S)-number of cycles (N) curve as the stress corresponding to 10^7 cycles. Fracture toughness tests were conducted at 25 °C in a computer-controlled 10 ton capacity "MTS-810" (MTS Systems Corporation, Minnesota, MN) model dynamic testing machine on 25 mm thick compact tension (CT) specimens (with chevron-type notch) per ASTM standard designation E 399-90. The CT specimens were prepared from the head portion of rails according to dimensions shown in Fig. 3. The samples were precracked up to a crack length (a) to test piece width (W) ratio, a/W, of 0.50 at 10 Hz frequency and stress intensity of the order of 20 MPa $\sqrt{m}$ at a stress ratio (*i.e.*, ratio of minimum stress to maximum stress), R, of 0.10. Precracked specimens were then tension tested by using a 12 mm crack opening displacement gauge. The dimensions of the fractured surface were measured and the final crack length was determined from the average values of measurements. For fracture toughness testing, five specimens were tested per heat and the average of three close values was reported. Since valid plane-strain fracture toughness (K_{Ic}) criteria could not be met, conditional K_Q values were calculated in accordance with ASTM standard designation E 399 - 90.

The fracture surfaces of tensile, fracture toughness, and fatigue-tested samples were examined visually for observing the general fracture topography. This was supplemented by extensive fractographic observations at higher magnifications in a JEOL make "JSM-840A" model scanning electron microscope. Qualitative analysis of inclusions observed on fracture surfaces, particularly at crack initiation sites, was carried out through energy dispersive spectrometric (EDS) analysis to identify inclusion chemistry.

3. Results and Discussions

3.1 Chemical Composition

The details of heat numbers and chemical composition (in wt.%) of the rail steels investigated are shown in Table 1. The chemical compositions of all six rail steel heats were found to be within the stipulated range mentioned under the "Indian Railway standard specification for flat bottom rails" (Sl.No. T-12-96) for 880 MPa (90 kg/mm^2) UTS grade rails.[6] It can be seen from this table that the carbon content in rail steel heat numbers 1, 3, 4, 5, and 6 ranged from 0.70 to 0.74 wt.%, while the carbon content (0.68 wt.%) in heat number 2 was the least. The manganese content of all the heats was found to be in a very close range and varied from 0.99 to 1.09 wt.%. The sulfur

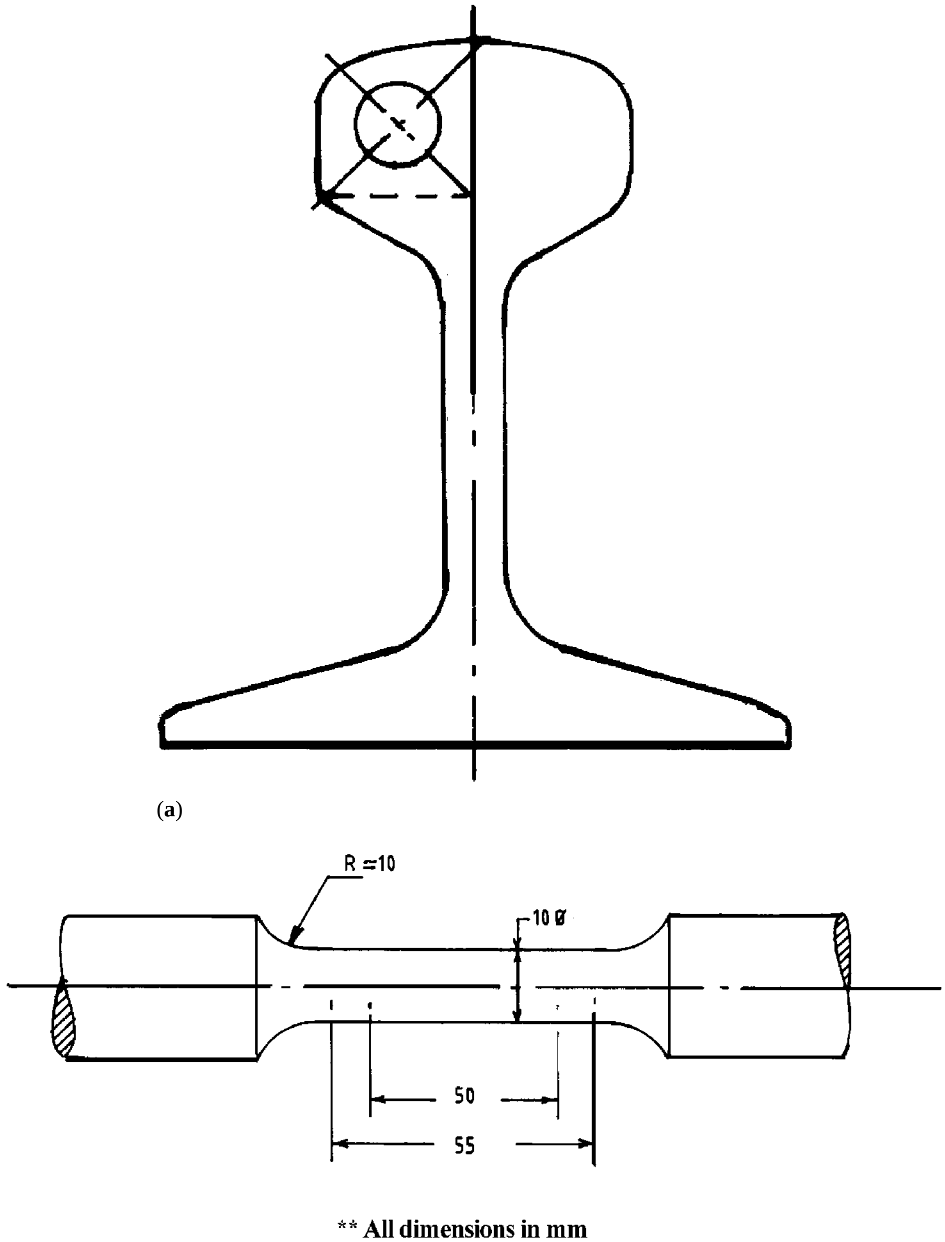

(b)

Fig. 1 (**a**) Rail section showing location of tensile test piece. (**b**) Dimensions of standard tensile test specimen

content in the six heats, however, varied between 0.020 and 0.033 wt.%, being least (0.020 wt.%) in heat number 2 and highest (0.033 wt.%) in heat number 1. Although the aforesaid railway standard specification permits a wide range (0.10 to 0.50 wt.%) for the silicon content, silicon in the investigated heats varied between 0.18 and 0.24 wt.%. The aluminum content in all six rail steel heats was found to be 0.01 wt.% against a stipulated maximum of 0.02 wt.%.

3.2 Macrostructure

The sulfur prints of all the rail sections investigated were satisfactory and did not reveal any noticeable sulfur segregation. The macroetched structure of the rail sections was also found to be satisfactory; no major cracks, piping, or other defects could be observed.

3.3 Inclusion Characteristics

The main types of NMI observed in the six rail heats are summarized in Table 2. In heat numbers 1, 2, and 6, manganese sulfide inclusions were mostly seen, while oxide inclusions along with sulfides could be observed in heat numbers 3, 4, and 5. The oxide inclusions in heat numbers 3, 4, and 5 might have possibly originated from deoxidation products and/or slag. Titanium nitride (TiN) inclusions of cubic morphology were

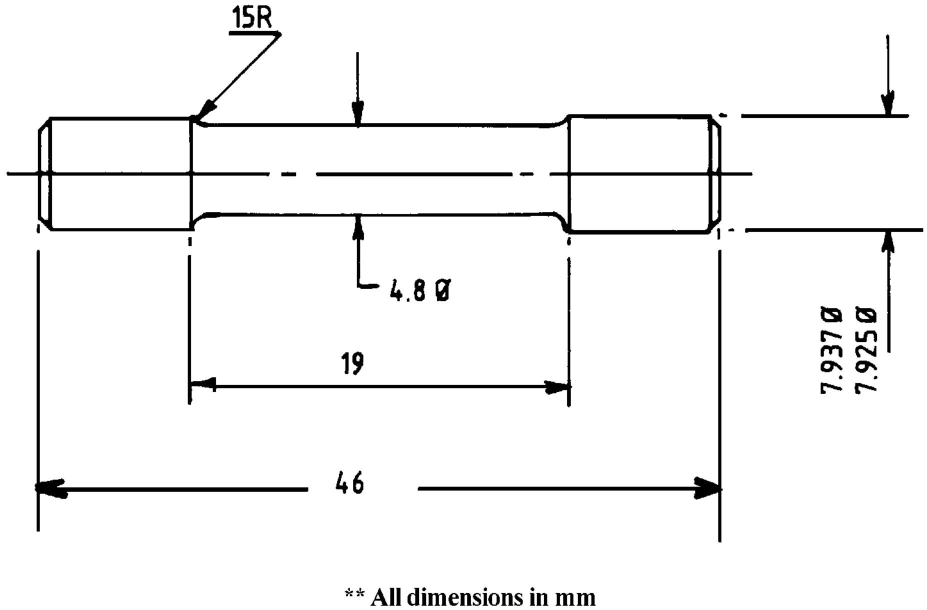

Fig. 2 Specimen geometry of high-cycle fatigue specimen

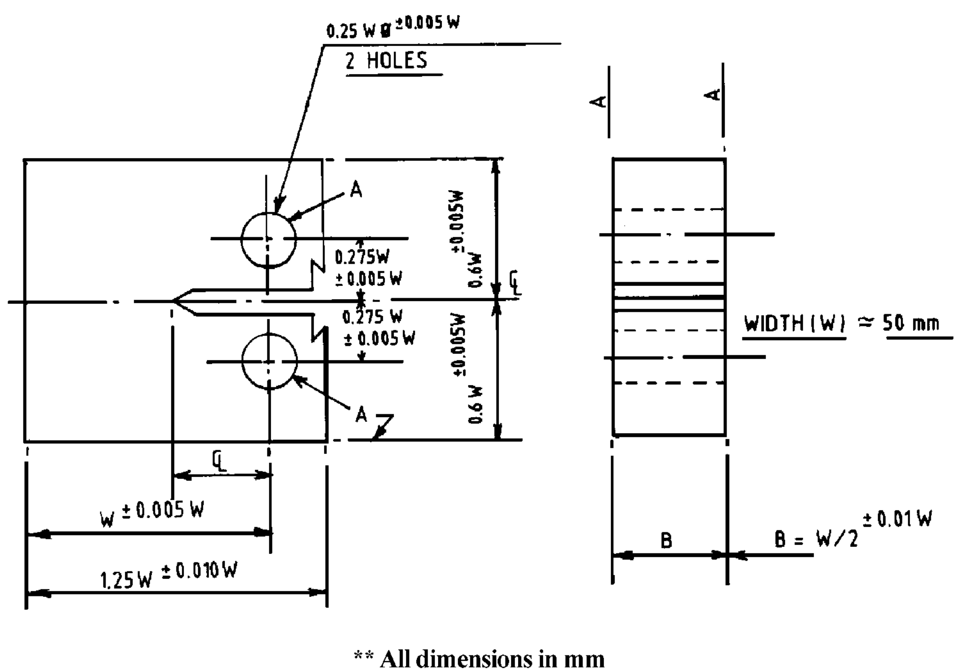

Fig. 3 Specimen geometry of CT specimen for fracture toughness evaluation

also observed in some of the rail heats. Titanium is a strong nitride former and its incidence might possibly be from the steel scrap added in the BOF. Optical micrographs showing typical inclusion fields observed in the six rail steel heats are shown in Fig. 4 to 6 at 500× magnification. It is clearly evident from Fig. 4(a) and (b) that although the majority of inclusions in heat numbers 1 and 2 are stringer-type sulfides, dispersions of few angular TiN inclusions are also seen. The presence of brittle alumina chains in addition to MnS inclusions is visible in a sample of heat number 3, as shown in Fig. 5(a) at 500× magnification. In heat number 4 (Fig. 5b), however, oxides enveloped by sulfides are seen in addition to arrays of ellipsoidal MnS inclusions. Heat number 5 showed a preponderance of thick and elongated sulfides (Fig. 6a), while oxide inclusions encapsulated by sulfides (Fig. 6b) were seen in heat number 6.

The average volume fractions (in percent) of NMI in each sample were determined by quantitative image analysis from measurements over 30 random fields and varied between 0.23

Table 1 Chemical composition of investigated rail steels

Heat number	Composition (wt.%)					
	C	Mn	Si	S	P	Al
1	0.70	1.09	0.20	0.033	0.022	0.01
2	0.68	1.00	0.24	0.020	0.018	0.01
3	0.71	0.99	0.22	0.025	0.025	0.01
4	0.74	1.00	0.18	0.026	0.019	0.01
5	0.72	1.02	0.20	0.030	0.017	0.01
6	0.72	1.05	0.22	0.023	0.020	0.01

Table 2 Microstructural characteristics of NMI in the investigated rail steels

Heat number	Characteristics of NMI
1	Inclusions mostly elongated and ellipsoidal sulfides, some of which were found to envelop oxides. TiN occurrence rare
2	Inclusions generally sparse. Sulfides mostly thin and elongated. Oxides, alumina, and silicates not observed
3	Inclusions mostly sulfides, some of which were associated with TiN. Alumina stringers observed at many places
4	Inclusions mostly ellipsoidal sulfides, some associated with oxide particles. Silicate stringers observed at few places
5	Inclusions mostly sulfides, some of which were embedded with oxides. TiN and alumina inclusions observed at few places
6	Inclusions mostly sulfides. Oxides and TiN rarely found

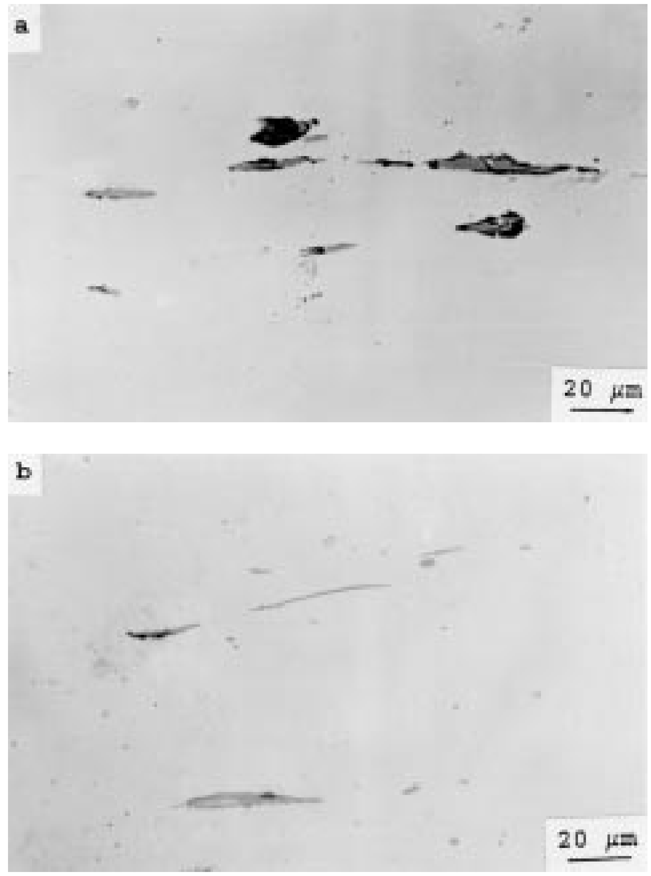

Fig. 4 Optical micrographs of typical inclusion fields in rail samples: (**a**) heat number 1 showing thick elongate and ellipsoidal sulfides and (**b**) heat number 2 showing thin elongated sulfides; 500×

and 0.45 (Table 3) in the rail steel heats. It can be seen from this table that the overall cleanliness decreases in the order of heat numbers 2, 6, 1, 4, 3, and 5. The average volume fractions of oxide and sulfide inclusions as determined by quantitative image analysis are also shown in Table 3. The volume fraction of sulfides is found to be lower in heat number 2 (0.15%) and heat number 6 (0.19%), while it is comparatively higher in the other four heats where it varies between 0.22 to 0.27%. Regarding oxide inclusions, their population is on the lower side in heat 1 (0.06%) and heat 2 (0.08%), while it is higher in the other four heats where it varies between 0.13 and 0.21 vol.%.

Electron-probe microanalysis (EPMA) of the various species of NMI observed in the six rail steel heats indicated that the sulfides were essentially pure MnS. The EPMA investigations of oxides enveloped by sulfides indicated that these were essentially alumina or calcium aluminate type inclusions. The orange-colored cube-shaped inclusions were corroborated by EPMA to be essentially TiN.

3.4 Microstructure

Optical metallography of nital-etched rail steel samples revealed fully pearlitic structure with slight amounts of proeutectoid ferrite precipitation along the prior austenite grain boundaries. The typical microstructures observed in samples of heat numbers 1 and 5 are shown in Figs. 7(a) and (b), respectively, at 500× magnification.

The pearlite interlamellar spacings in all six rail steel heats were measured from the microphotographs of polished and etched samples observed by SEM. The average pearlite interlamellar spacings in the six rail steel heats investigated varied between 0.22 and 0.33 μm. These values of interlamellar spacing are quite normal in pearlitic rail steel.[7] Typical SEM micrographs showing pearlite interlamellar spacing in samples of heat numbers 1 and 4 are shown in Figs. 8(a) to (d) at 5000× and 10,000× magnifications. The average interlamellar spacings depicted in the aforesaid micrographs were found to be 0.249 and 0.312 μm for samples of heat numbers 1 and 4, respectively.

3.5 Mechanical Properties

Tensile Properties. The tensile properties (YS, UTS, and elongation) of the six rail steel heats investigated are shown in Table 4. The UTS and elongation values obtained in all these heats were found to be above the minimum stipulated requirements of 880 MPa and 10%, respectively, for 90 kg/mm^2 UTS grade of rail steel.[6] The YS values in the six rail steel heats varied from 454 to 495 MPa, while the UTS values were found to range from 893 to 934 MPa. The elongation values (on 50 mm gauge length), on the other hand, ranged between 10.55 and 11.85%. From the tensile property data in Table 4, it is observed that heat number 2, which exhibited the lowest UTS (893 MPa), showed the maximum (11.85%) elongation. This heat incidentally has the lowest carbon (0.68 wt.%) content.

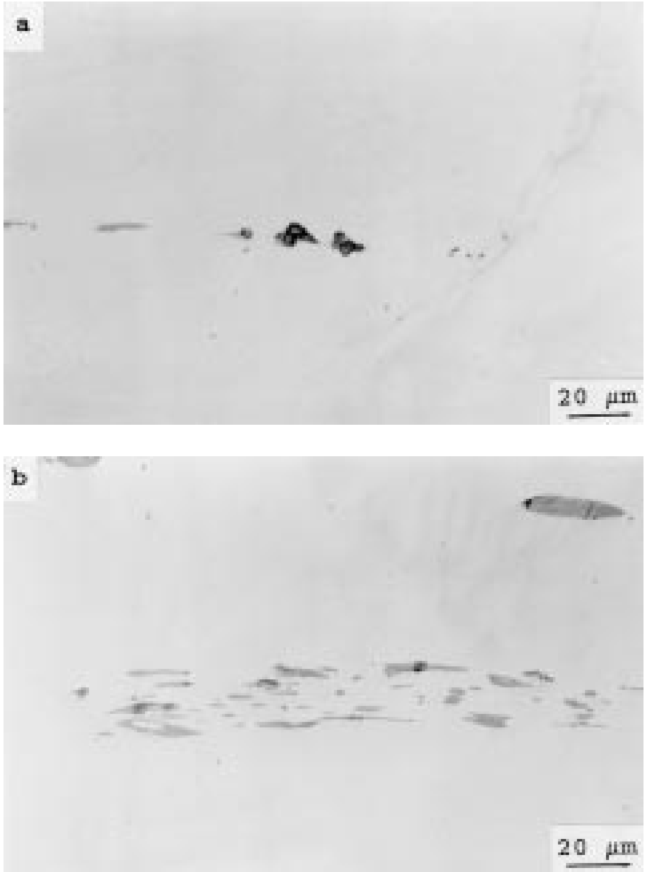

Fig. 5 Optical micrographs of typical inclusion fields in rail samples: (**a**) heat number 3 showing thin elongated sulfide and alumina stringer and (**b**) heat number 4 showing parallel bands of small elongated sulfides and oxysulfides; 500×

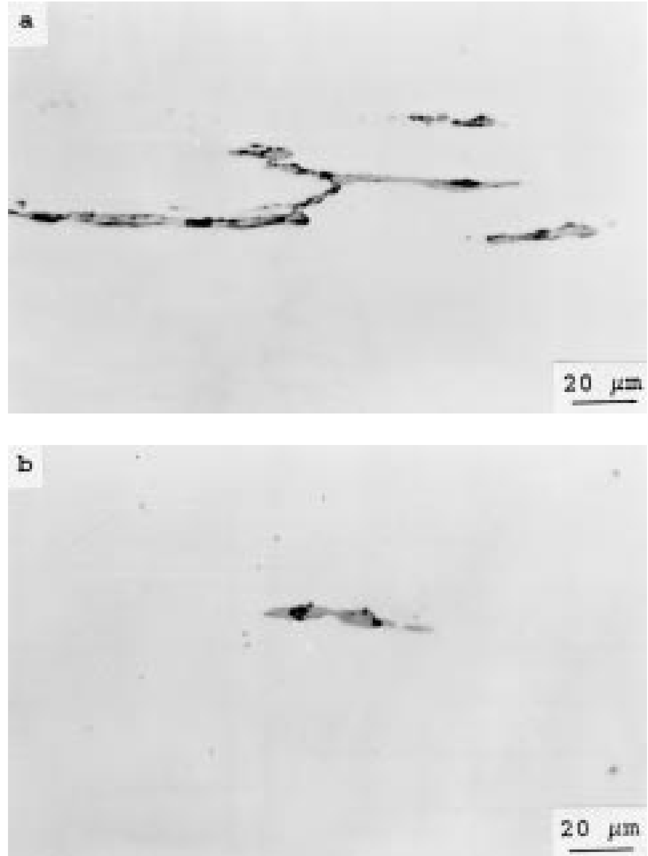

Fig. 6 Optical micrographs of typical inclusion fields in rail samples: (**a**) heat number 5 showing fork-shaped thick sulfide stringer and (**b**) heat number 6 showing elongated sulfide with entrapped oxide; 500×

However, it is observed that the present level of total inclusions (0.23 to 0.45 vol.%) and their type have no definite influence on the YS, UTS, and elongation values in the investigated rail steels.

Fracture Toughness. The conditional fracture toughness (K_Q) values (Table 4) obtained in the six rail heats were found to vary between 42.33 and 49.88 MPa $\sqrt{m}$. Although the fracture toughness values obtained in all the heats were found to be above the minimum stipulated requirement of 42 MPa $\sqrt{m}$, high fracture toughness (K_Q) values (49.88 and 46.72 MPa $\sqrt{m}$) were obtained for samples of heat numbers 2 and 6. In the other four heats, the K_Q values were lower and ranged between 42.33 and 43.87 MPa $\sqrt{m}$. It is interesting to observe that heat numbers 2 and 6, which exhibited higher fracture toughness (K_Q) values, showed (Table 3) lower volume fractions (0.15 and 0.19%, respectively) of sulfide inclusions. The other four heats (1, 3, 4, and 5), however, showed higher sulfide volume fractions (0.22 to 0.27%), being particularly high in heats 1 and 5, which exhibited comparatively lower K_Q values. This presumably indicates the beneficial effect of lower sulfide volume fraction in improving fracture toughness. Yongliang *et al.*,[8] in their studies on rail steels, reported a similar trend. According to them, the K_{Ic} value of rail steel is related to the UTS and average density of sulfide inclusions; *i.e.*, the fracture toughness value would decrease with increase in UTS and average density of sulfides. This phenomenon is understandable because cracks are initiated preferentially at the sulfide inclusion-steel matrix interface and propagate successively along strip-shaped inclusions with increase in load. Subsequently, transverse cracks generate from the initial longitudinal cracks, leading to microcracking in steel. This is possibly the reason why the K_{Ic} value of steel can be reduced by a higher sulfur content and the preponderance of stringer-type sulfides.

Table 3 Volume fractions of NMI in investigated rail steels

	Inclusion volume fraction (%)		
Heat number	**Sulfide**	**Oxide**	**Total**
1	0.27	0.06	0.33
2	0.15	0.08	0.23
3	0.22	0.21	0.43
4	0.23	0.15	0.38
5	0.26	0.19	0.45
6	0.19	0.13	0.23

Typical photographs of fractured CT specimens of heat numbers 1 and 2 are shown in Fig. 9(a) and (b), respectively. It can

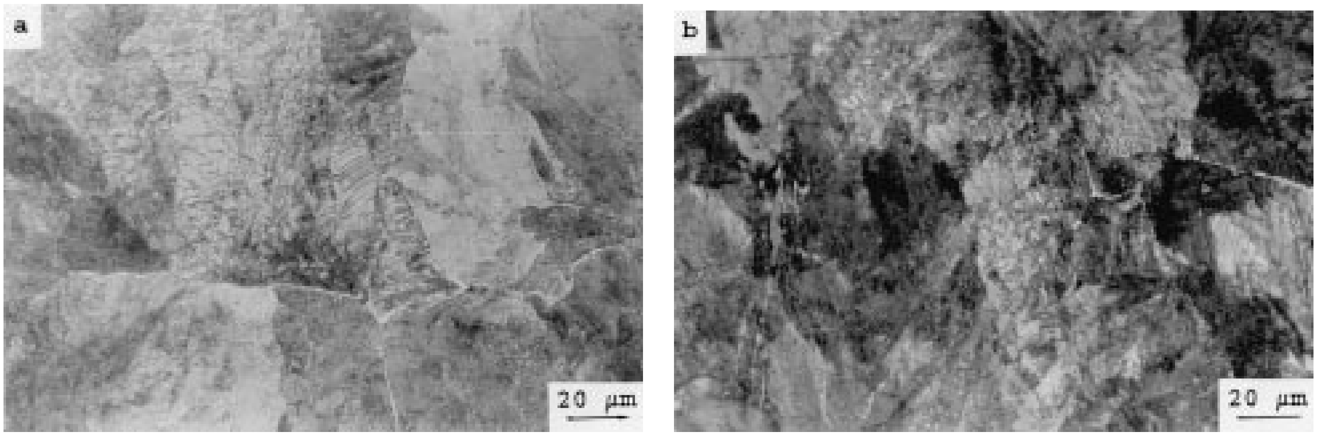

Fig. 7 Typical pearlitic microstructure with a small amount of proeutectoid ferrite in rail steels: (**a**) heat number 1 and (**b**) heat number 5; 500×

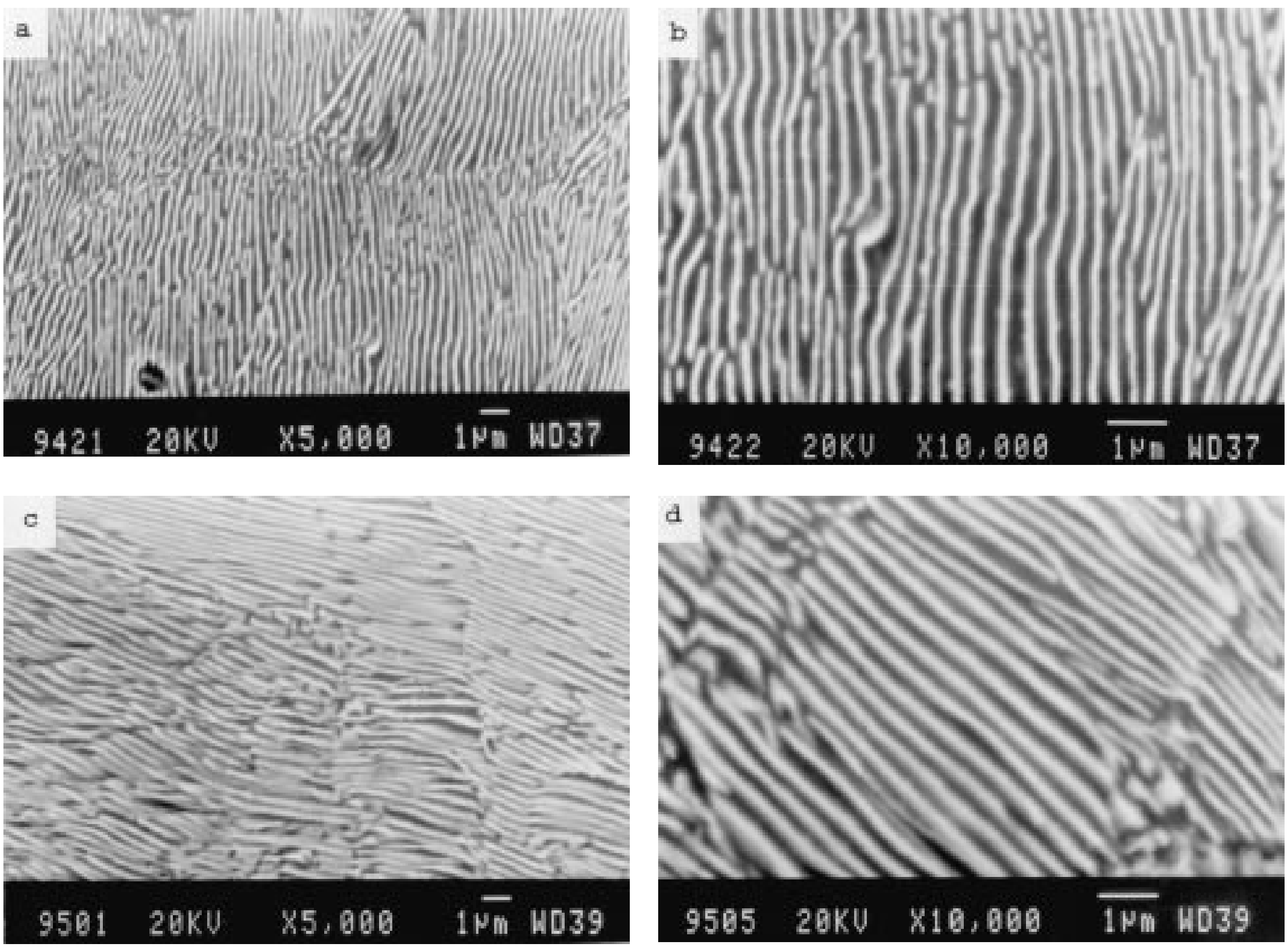

Fig. 8 SEM images showing resolved pearlite lamellae in rail steels: (**a**) heat number 1, 5000×; (**b**) heat number 1, 10,000×; (**c**) heat number 4, 5000×; and (**d**) heat number 4, 10,000×

be clearly seen from these photographs that the proportion of ductile area in the precracked zone of the tested specimen of heat number 1 is significantly lower than that observed in the specimen of heat number 2. This is in agreement with their respective fracture toughness values (Table 4); *i.e.*, $K_Q = 42.33$ and 49.88 MPa $\sqrt{m}$.

High-Cycle Fatigue Properties. The high-cycle fatigue limits (Table 4) obtained in the six rail steel heats varied between

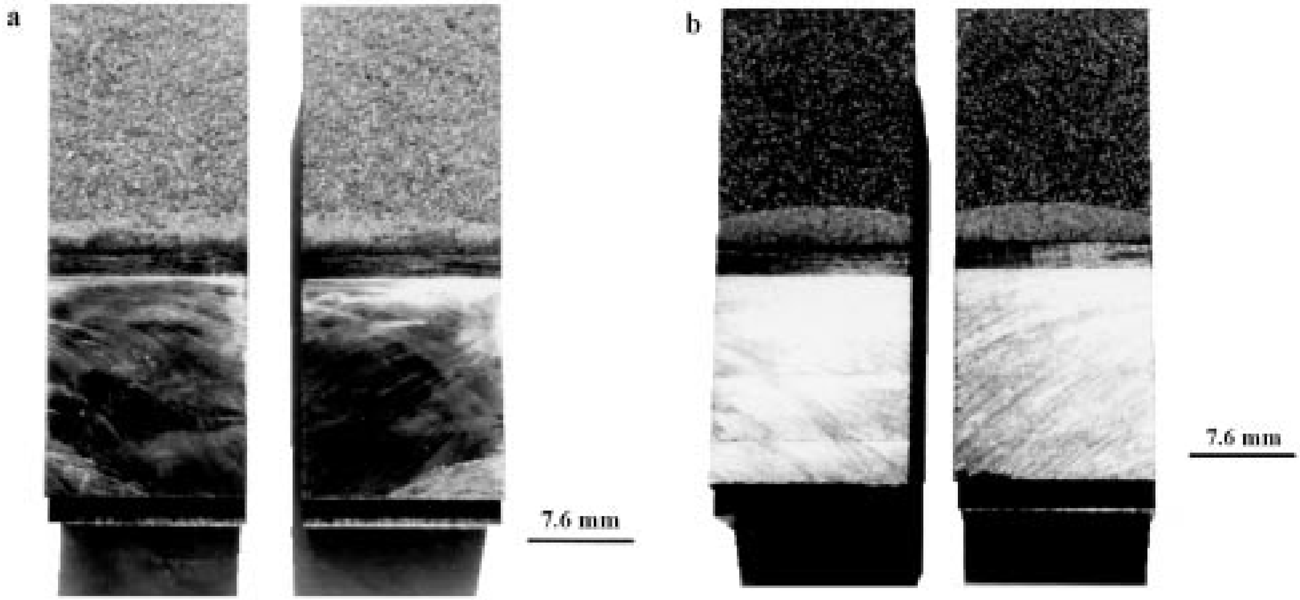

Fig. 9 Typical photographs of fractured CT specimens showing (**a**) less ductile area in specimen of heat number 1 and (**b**) more ductile area in specimen of heat number 2

Table 4 Mechanical properties of investigated rail steels

Heat number	Tensile Properties YS (MPa)	UTS (MPa)	Elongation (%)	Fracture toughness (MPa $\sqrt{m}$)	Fatigue strength (MPa)
1	484	908	10.70	42.33	355
2	468	893	11.85	49.88	350
3	490	906	10.70	43.87	319
4	454	909	11.40	43.85	335
5	495	934	11.00	42.81	320
6	464	900	10.55	46.72	343

319 and 355 MPa. It can be observed from this table that the fatigue limit decreases in the order of heat numbers 1, 2, 6, 4, 5, and 3. As a matter of fact, the fatigue limits exhibited by samples of heat numbers 3, 4, and 5 appear to be on the lower side, *i.e.*, 319 to 335 MPa. Interestingly, the aforesaid three heats are also extremely dirty from the standpoint of total inclusion volume fraction, *i.e.*, 0.38 to 0.45%. Heat numbers 1, 2, and 6, which exhibit higher fatigue limits (343 to 355 MPa), are found to be comparatively cleaner with respect to the total inclusion content. The relationship of fatigue limit with the level of sulfide inclusions, however, is not clear from our study. However, the fatigue limits (Table 4) achieved in the investigated steels seem to have a direct correspondence with the volume fraction of oxide inclusions (Table 3), as shown in Fig. 10. This is understandable since brittle oxide inclusions such as alumina and calcium-aluminates are nondeformable and act as stress raisers[8,9] to serve as crack initiation sites. Under applied stresses, these cracks propagate and culminate in failure. Although it is generally believed that fatigue limit increases in higher yield strength steels,[10] no such trend has been evident in our studies. Similar nonconformity of fatigue limit with yield strength has also been reported by Liu *et al.* in their investigations on fatigue crack initiation of fully pearlitic steels.[11]

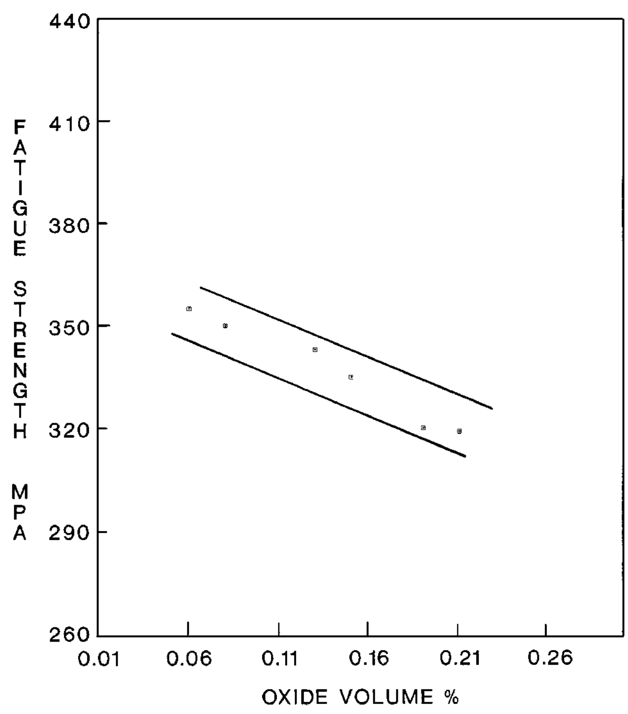

Fig. 10 Plot showing variation of fatigue strength with oxide inclusion content in investigated rail steels

The SEM photographs showing the fracture topography of fatigue-tested specimens of heat numbers 2 and 3 are shown in Fig. 11(a) and (b), respectively, at 1000× magnification. It

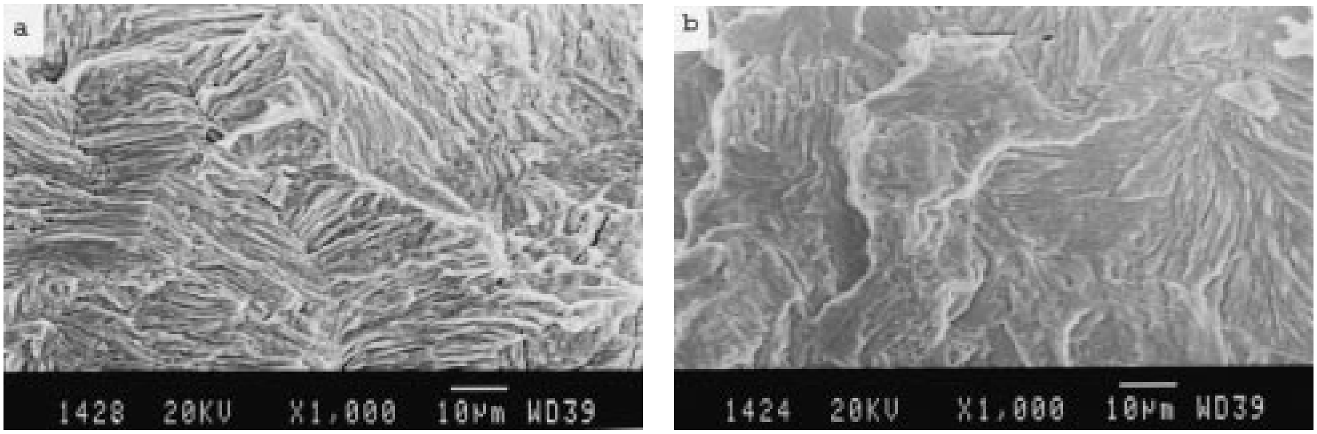

Fig. 11 SEM fractographs of fatigue-tested rail steel specimens showing (**a**) numerous fatigue striations in heat number 2 and (**b**) lower density of fatigue striations in heat number 3; 1000×

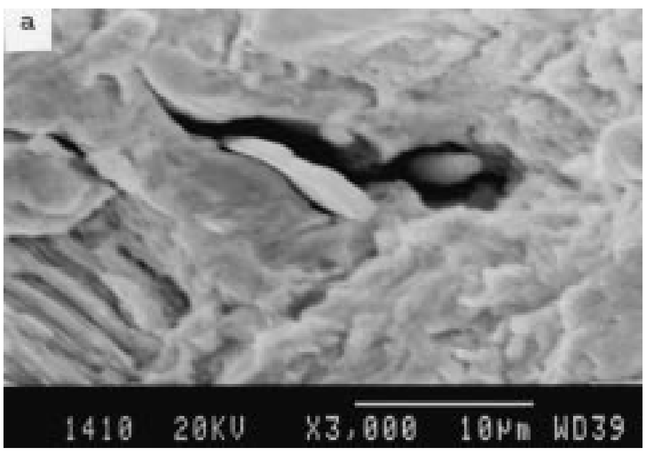

(**a**)

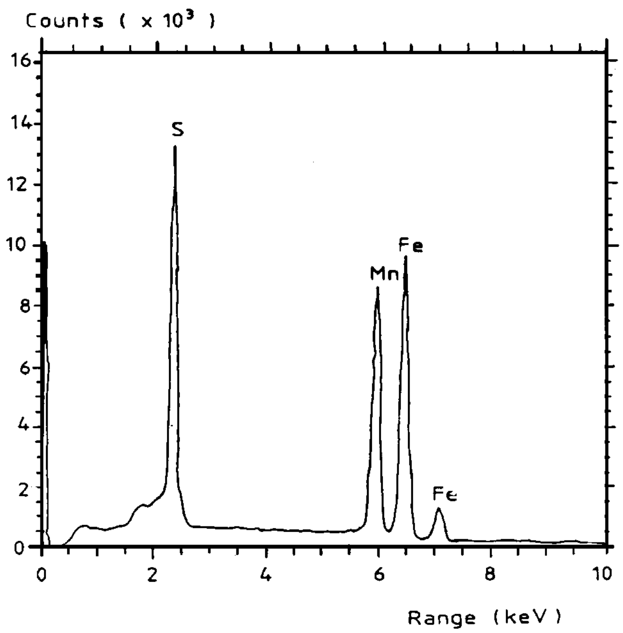

(**b**)

Fig. 12 (**a**) SEM fractograph of the fatigue-tested specimen of heat number 1 showing elongated MnS inclusion at crack initiation site, 3000×; and (**b**) EDS spectrum of the same inclusion

can be clearly seen that while the fracture surface in Fig. 11(a) shows numerous fatigue striations, a lower density of striations is observed in Fig. 11(b). The higher density of striations in Fig. 11(a) is in agreement with the higher fatigue limit of heat number 2. Figure 12 and 13 show inclusion-assisted cracking in the fracture surfaces of fatigue-tested samples of heat numbers 1 and 4, respectively. Although it is generally believed that sulfide inclusions are relatively less harmful than hard and nondeformable oxides, our studies have elucidated the role of MnS inclusions in initiating cracks. The SEM fractograph in Fig. 12(a) shows debonding at the interface between the matrix and an elongated inclusion at 3000× magnification. The EDS analysis (Fig. 12b) confirmed the elongated inclusion to be pure MnS. The Fe peak in the EDS spectrum is attributed to matrix excitation. The fatigue cracking in this sample seems to have initiated at the tip of the elongated MnS inclusion. The SEM photograph showing an oxide inclusion and cracking on the fracture surface of a fatigue-tested specimen of heat number 4 is shown in Fig. 13(a) at 2000× magnification. The EDS spectrum (Fig. 13b) of the same inclusion shows that the inclusion is basically a complex oxide of Ca, Al, Si, Mn, and Fe. This inclusion chemistry is suggestive of slag genesis. The spherical morphology of this oxide inclusion is indicative of brittleness and a low index of deformability. Unlike plastic

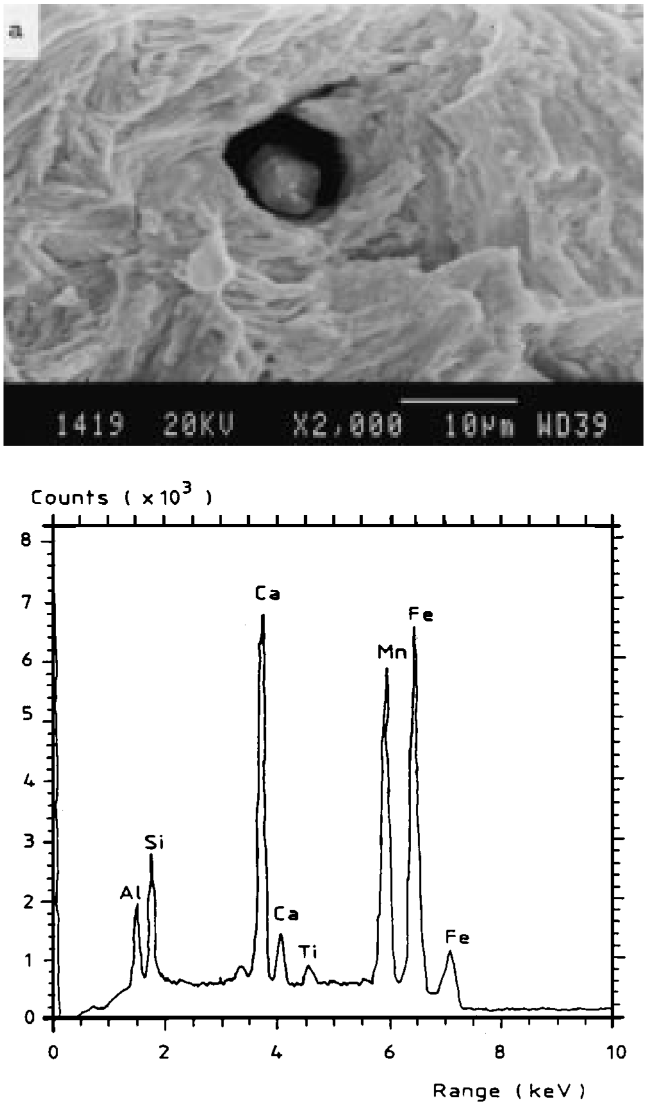

(**b**)

Fig. 13 (**a**) SEM fractograph of the fatigue-tested specimen of heat number 4 showing complex oxide inclusion at crack initiation site, 2000×; and (**b**) EDS spectrum of the same inclusion

sulfide inclusions, where cracking is associated with inclusion-matrix decohesion, brittle and nondeformable oxide inclusions may themselves break to act as cracks.

4. Conclusions

- The rail steels investigated were macrostructurally sound and did not exhibit any noticeable segregation. Microstructurally, all rail specimens exhibited fully pearlitic structures with negligible ferrite precipitation. The interlamellar spacings of pearlite were found to range between 0.21 and 0.33 μm, which is normal for pearlitic rail steel.
- The volume fractions of NMI in the investigated rail steel heats varied between 0.23 and 0.45%. Inclusions were mostly MnS, some of which were found to envelop oxides. Al_20_3 stringers, globular oxides, and TiN were also found in some of the heats.
- The tensile properties (YS, UTS, and elongation) of the investigated steels were found to be insensitive to inclusion type and content at the present volume fraction levels.
- The conditional fracture toughness (K_Q) values were found to range between 42.33 and 49.88 MPa $\sqrt{m}$; higher values, in general, were obtained in heats exhibiting lower volume fractions (0.15 to 0.19%) of sulfide inclusions.
- The high-cycle fatigue limits were found to range between 319 and 355 MPa; higher values were obtained in cleaner steels, particularly in those with lower volume fractions of oxide inclusions. Although fatigue life did not show any direct correlation with sulfide volume fraction, SEM investigations showed that elongated MnS inclusions were sometimes observed at crack initiation sites of fatigue-tested specimens.

Acknowledgments

The authors acknowledge with gratitude the support and encouragement provided by the management of the R&D Centre for Iron and Steel (RDCIS), Steel Authority of India Limited (Ranchi), for pursuing this study. Thanks are expressed to the personnel of the metallography and mechanical testing laboratories at RDCIS for their help in the investigation and to Mr. B. Khalkho for typing the manuscript in a short span of time.

References

1. H. Schmedders and K. Wick: *Rail Steels Symp. Proc.*, Iron and Steel Society, Warrendale, PA, 1992, pp. 35-48.
2. J.H. Martens and D.P. Wirick: *Rail Steels Symp. Proc.*, Iron and Steel Society, Warrendale, PA, 1994, pp. 3-5.
3. A. Ray, S.K. Dhua, and S. Jha: *X-Ray Spectr.*, 1999, vol. 28 (1), pp. 41-50.
4. A.B. Dobuzhskaya, V.A. Reikhart, V.I. Syreishchikova, A.V. Veliakanov, and I.V. Koshina: *Steel USSR*, 1990, vol. 20 (11), pp. 561-64.
5. P.G. Forrest: *Fatigue of Metals*, Pergamon Press, Oxford, United Kingdom, 1970, pp. 12-55.
6. Indian Railway Standard Specification for Flat Bottom Rails Serial No. T-12-96, issued by Research Designs and Standards Organisation, Lucknow.
7. C.D. Liu, M.N. Bassim, and S. St. Lawrence: *Mater. Sci. Eng. A*, 1993, vol. A167 (1–2), pp. 107-13.
8. Y. Yongliang, S. Kangying, C. Yinzhi, and W. Chunming: *HSLA Steels: Processing, Properties and Applications Conf. Proc.*, TMS, Warrendale, PA, 1990, pp. 451-56
9. D. Brooksbank and K.W. Andrews: *J. Iron Steel Inst.*, 1972, vol. 210 (4), pp. 246-55.
10. G.T. Gray, A.W. Thompson, and J.C. Williams: *Metall. Trans. A*, 1985, vol. 16A, pp. 753-59.
11. C.D. Liu, M.N. Bassim, and S. St. Lawrence: *Eng. Fract. Mech.*, 1995, vol. 50 (2), pp. 301-07.